International Journal of Mass Spectrometry 279 (2009) 5–9

Contents lists available at ScienceDirect

International Journal of Mass Spectrometry

journal homepage: www.elsevier.com/locate/ijms

A novel design of a temperature-controlled FT-ICR cell for low-temperature black-body infrared radiative dissociation (BIRD) studies of hydrated ions

O. Petru Balaj[a,1], Christian B. Berg[b], Stephan J. Reitmeier[a], Vladimir E. Bondybey[a], Martin K. Beyer[a,c,*,1]

[a] Department Chemie, Lehrstuhl 2 für Physikalische Chemie, Technische Universität München, Lichtenbergstraße 4, 85747 Garching, Germany
[b] Bruker Daltonics, Inc., 40 Manning Road, Billerica, MA 01821, USA
[c] Institut für Physikalische Chemie, Christian-Albrechts-Universität zu Kiel, Olshausenstrasse 40, 24098 Kiel, Germany.

ARTICLE INFO

Article history:
Received 7 July 2008
Received in revised form 1 September 2008
Accepted 2 September 2008
Available online 10 September 2008

Keywords:
Molecular clusters
Black-body radiation
FT-ICR mass spectrometry
Intracluster reactions

ABSTRACT

A novel design for a temperature-controlled ICR cell is described for use in black-body infrared radiative dissociation (BIRD) studies of weakly bound systems like water clusters. Due to several improved design features, it provides a very uniform black-body radiation environment, and at the same time maintains efficient pumping for a low collision rate on the order of 10^{-2} s^{-1}. At the lowest temperatures reached, nominally 89 K cell plate temperature, water evaporation effectively ceases, while intracluster reactions in $V^+(H_2O)_n$ with a small activation energy are still observed. BIRD rate constants for $Ag^+(H_2O)_n$, $n = 4$–6, are shown in the temperature range $T = 160$–320 K. For $n = 6$, a linear Arrhenius plot with $R^2 = 0.9943$ is obtained without any calibration, confirming the suitability of the cell for quantitative BIRD studies.

1. Introduction

McMahon and coworkers reported unimolecular dissociation reactions of weakly bound ionic clusters, and concluded that the energy necessary for dissociation was absorbed from ambient black-body radiation [1]. Similar observations have been made by several groups, who all confirmed the initially hotly debated finding [2–15]. It was soon realized that quantitative information on activation energies can be extracted from a measurement of unimolecular rate constants as a function of temperature. However, only if the ion is in the rapid energy exchange limit [16], an Arrhenius plot will directly yield activation energies. In all other cases, i.e., if energy exchange via emission and absorption of infrared photons is not much faster than dissociation, master equation modeling must be applied to account for the rates of photon absorption and emission in the ensemble of ions [3,7]. A detailed account of all aspects of black-body infrared radiative dissociation (BIRD), a term introduced by Williams and coworkers [6], as well as master equation modeling, is given in a recent review by Dunbar [17].

Most BIRD experiments have been performed from room temperature up to 523 K. This temperature range allows the study of systems with bond strengths in the range 70–200 kJ/mol [17]. To achieve the desired temperatures, heated filaments were placed close to the cell excitation–detection plates [18–20] or simply the infrared radiation from a directly heated vacuum chamber [21] was used. Although the temperature of the filaments can be quite high, the temperature of the absorbed infrared radiation is anisotropic, i.e., the radiation temperature experienced by the ions is not well defined.

Weakly bound clusters like water clusters dissociate rapidly at room temperature, and further heating makes the rates too fast for the time scale of an ICR experiment. To extract quantitative information from BIRD experiments of water clusters, cooling of the black-body radiation environment must be accomplished. There are two liquid-nitrogen cooled ICR cells documented in the literature, which have been constructed to optimize two counteracting aspects. The cell developed by Heeren and coworkers in Amsterdam is an open ICR cell enclosed in a cylindrical ceramic cooling jacket [22], which optimizes pumping efficiency. It is ideally suited for combining radiative cooling of large molecular ions with SORI CID, which requires repeated gas pulses [23]. Due to the large solid angle which is open to room temperature black-body radiation, however, it does not provide a uniform low-temperature environment for quantitative BIRD experiments.

* Corresponding author. Tel.: +49 431 880 2831; fax: +49 431 880 2830.
E-mail address: beyer@phc.uni-kiel.de (M.K. Beyer).
[1] Current Address: Institut für Physikalische Chemie, Christian-Albrechts-Universität zu Kiel, Olshausenstrasse 40, 24098 Kiel, Germany.

1387-3806/$ – see front matter © 2008 Elsevier B.V. All rights reserved.
doi:10.1016/j.ijms.2008.09.001

Williams and coworkers developed a cell which hermetically closes the interior of the ICR cell with a solid, liquid-nitrogen cooled copper shield [14]. Room temperature contributions to the black-body radiation environment are minimized, but pumping is inefficient, since the volume inside the cell is evacuated only through two small orifices. The cell has been used successfully in the last years to study radiative dissociation of hydrated doubly and triply charged metal ions [14,24,25] and hydrated biomolecular ions [15,26,27]. The directly measured temperature of the cells walls is calibrated before it is used in master equation modeling [14], and the calibrated temperatures differ significantly from the originally measured values.

In the development of our ICR cell, we aimed at merging the two previous approaches in order to build a cell with the best possible compromise between pumping efficiency and black-body radiation shielding, since both factors are necessary to obtain accurate BIRD rate constants for water clusters at low temperatures.

2. Construction details of the novel design of a temperature-controlled ICR cell

A schematic diagram of the new ICR cell can be seen in Fig. 1. It is based on a Bruker "infinity" cell [28] which has been modified to allow for a spatially uniform temperature distribution. The original electrically and thermally insulating glass ceramics which mechanically support the cell have been replaced by high heat conductivity ceramics, an aluminum/boron nitride composite material distributed under the name SHAPAL-M soft (Tokuyama). It has a thermal conductivity of $90\,W\,m^{-1}\,K^{-1}$ at 25 °C, compared to $401\,W\,m^{-1}\,K^{-1}$ for copper. Unlike pure aluminum nitride, Shapal-M soft is machinable with standard tools. The SHAPAL-M soft parts are placed above the upper trapping plate, below the lower trapping plate, and two rings sustain the excitation/detection plates. To minimize heat transfer between the cell and the cell flange, a glass ceramics (Macor) mount with a thermal conductivity of $1.46\,W\,m^{-1}\,K^{-1}$ is replacing the original aluminum mount.

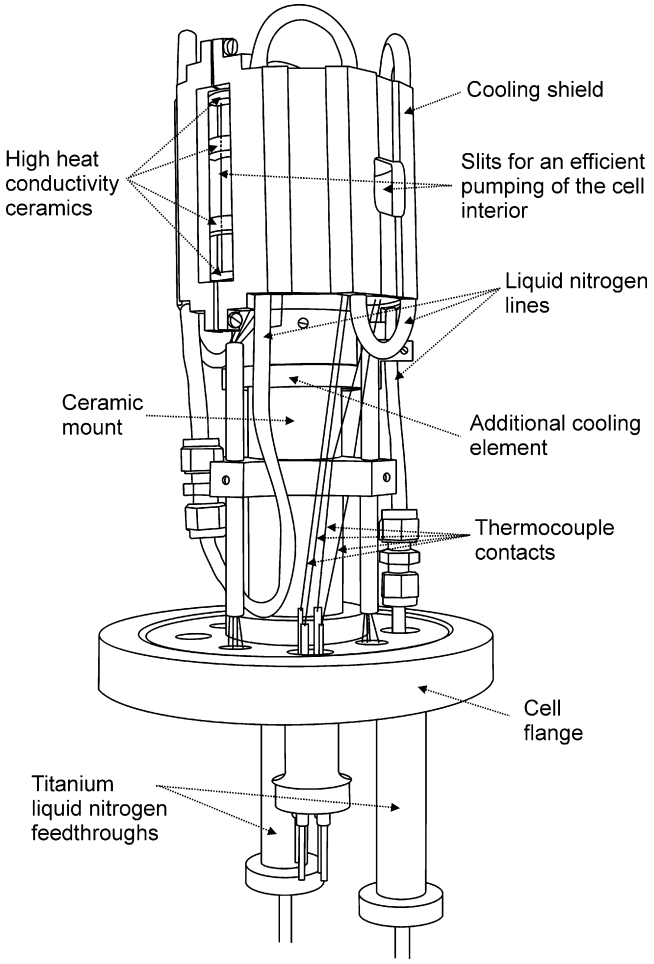

Fig. 1. Drawing of the temperature-controlled ICR cell.

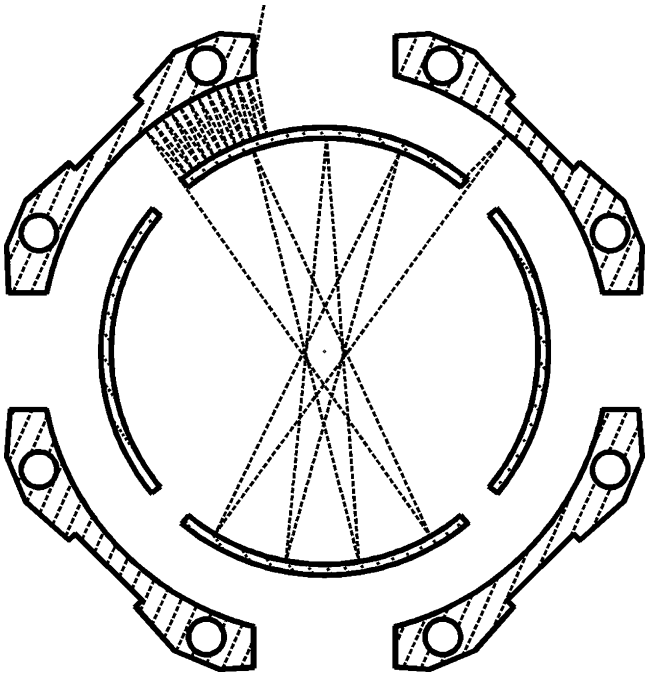

Fig. 2. Cross-section of the baffling geometry. The dashed line sketches the pathway of incoming room temperature black-body radiation which is coming as close as possible to the center of the cell. In each reflection, a fraction of the radiation is absorbed.

The cell is cooled either by liquid nitrogen, cold nitrogen gas, or heated nitrogen gas, depending on the desired temperature range. The coolant flows through 4-mm i.d. channels drilled into a massive copper (oxygen free) shield, which are connected by loops of 6-mm copper tubing. The cooling shield "embraces" the cell fulfilling two objectives: to shield the cell from black-body radiation coming from the ultra-high vacuum chamber walls and to cool down the cell itself. The shield covers all the openings between the excitation, detection, and trapping plates of the original "infinity" cell, as illustrated in Fig. 2, which shows a cross-section of the cell. At the same time the shield does not hinder the pumping of the cell interior by leaving ample openings in places where the plates of the original cell are present. These design changes insure a uniform and rapid cooling of the excitation, detection and trapping plates. Room temperature radiation, which may enter the cell through the slits in the shield, is reflected into the cell on pathways which do not intersect with the cell axis, where the ions are aligned. The closer the paths get to the cell axis, the higher the number of reflections gets. Since with each reflection, a fraction of the light is absorbed, the contribution of room temperature photons entering through the slits in the shield to black-body radiation activation will be negligible. If the number of reflections is small, the light path is far from the axis. If the light path is close to the axis, the number of reflections is high, and most of the radiation is absorbed before it enters the cell.

During the initial tests a temperature gradient on the order of 10 K along the cell was observed, twice the desired upper limit of 5 K. Obviously, the heat flow through the glass ceramics mount caused this gradient between the two measurement points close to the center of the upper and lower trapping plate. To mitigate this problem, an additional copper cooling element was included which connects the upper end of the glass ceramics mount to the coolant inlet tube. As a consequence, the gradient along the cell decreased below 5 K over the full temperature range.

Similar to the two earlier designs [14,22], the supply lines for the coolant go through the cell flange. In order to avoid ice formation in the region of the preamplifier, special titanium feed-throughs for the coolant lines were built, extending the UHV region until well out of the preamplifier area. They are coupled to vacuum insulated lines (actively pumped to $\sim 10^{-2}$ mbar) which lead the coolant into and out of the magnet. The connection point between the two lines, located in the magnet, is electrically heated to 30 °C.

The temperature of the cell is monitored by two E-type thermocouples, which are mounted between the trapping plates and the corresponding Shapal-M soft ceramics, close to the axis of the cell. In this way, the maximum temperature gradient along the cell is measured. The thermocouples are connected to the auxiliary sensor module of the Bruker BVT 3300 DIGITAL unit used to control the flow of cold nitrogen gas through the copper shield. Cold nitrogen gas is supplied by controlled evaporation of liquid nitrogen from a storage Dewar. The BVT unit communicates via a RS323 serial interface with a PC computer running LabView [29]. The home-written software controls the nitrogen evaporation rate and records and displays the temperature of the cell, the liquid nitrogen level, the evaporator power and the status of the BVT3300 unit.

Both trapping plates have 6-mm wide orifices to allow ions or electrons from an optionally heated filament entering the trap. The cell is 78 mm long on the outside, leaving a 60 mm long cylindrical space inside for the ions. In the center of the cell, room temperature black-body radiation therefore covers a fraction of 0.2% of the full solid angle. Combined with the T^4-dependence of the total flux of black-body radiation, room temperature contributions increase the total flux by 1.0% at 200 K, 3.3% at 150 K and 16% at 100 K. Quantitative BIRD should be possible without further corrections to below 200 K, possibly down to the 150 K region. For systems which require temperatures below 150 K, corrections may be included in the master equation model to account for the contribution of room temperature black-body radiation.

3. Cooling behavior of the cell

The thermal behavior of the cell was characterized in a series of test experiments in a separate vacuum chamber. With cold nitrogen gas from the evaporator, the cell can be operated in the 135–300 K temperature range. With liquid nitrogen, trapping plate temperatures of 89 K are reached. The temperature of the cell is controlled via the amount of nitrogen gas generated by the evaporator. In the tests, the evaporator power was gradually raised from 0% to 100% and the ICR cell temperature was recorded. The temperature decrease was done in steps of 10% liquid nitrogen heater power to decrease the risk of structural damage to the cell. As shown in Fig. 3, there is a sharp initial decrease of the temperature following each such step. Within 20 min, the temperature will reach a steady value which can be maintained for a long time. The curves in the panel (b) of the figure show that the lowest temperature reached in the test stand was 135 K at 100% heater power. The temperatures shown in Fig. 3 represent both cell thermocouples connected to channel 0 and channel 1 of the BVT 3300 unit. The temperature difference between the two channels reveals a temperature gradient along

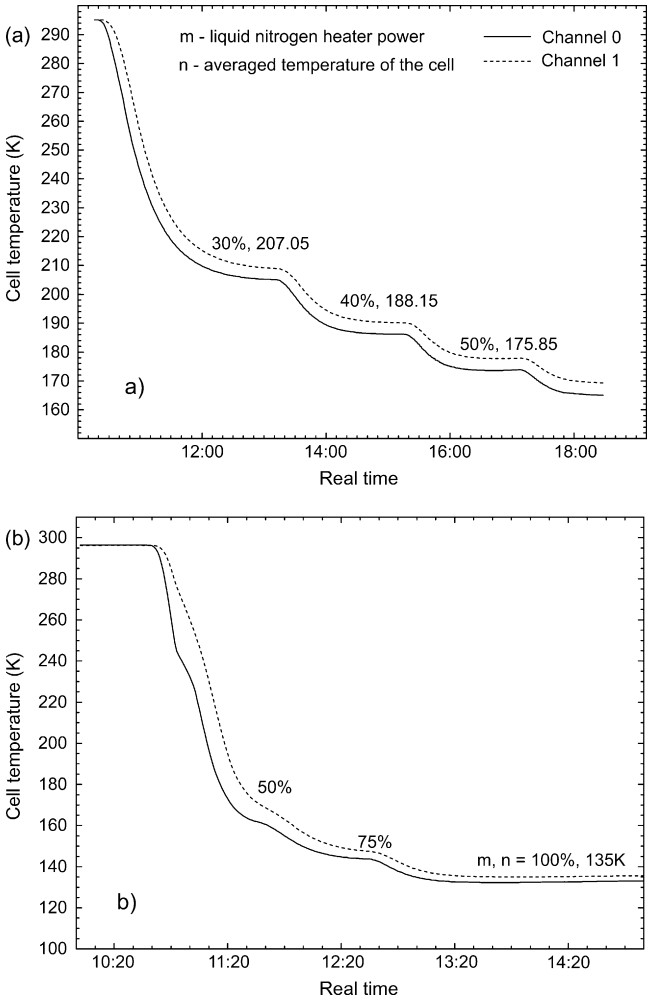

Fig. 3. Temperature–time behavior of the cell using the evaporator. The cell temperature depends directly on the liquid nitrogen heater power. In panel (a) the heater was powered initially to 30%, the time needed for the temperature to stabilize and the final temperature were measured. Once the temperature stabilized, the power was increased to 40% then 50%. Panel (b) shows the lowest temperature that can be obtained for 100% heater power, 135 K. To avoid any structural damage in a very fast cooling process the decrease of the temperature was done in steps, first using a 50% and then 75% heater power.

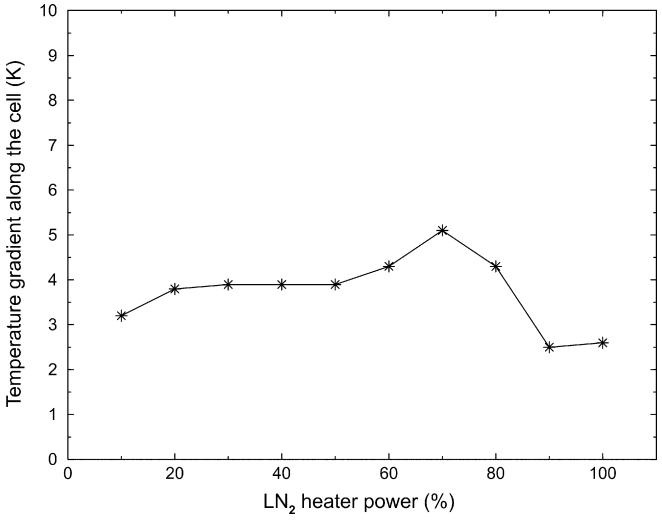

Fig. 4. The dependence of the temperature gradient along the cell on the liquid nitrogen heater power in the high temperatures regime.

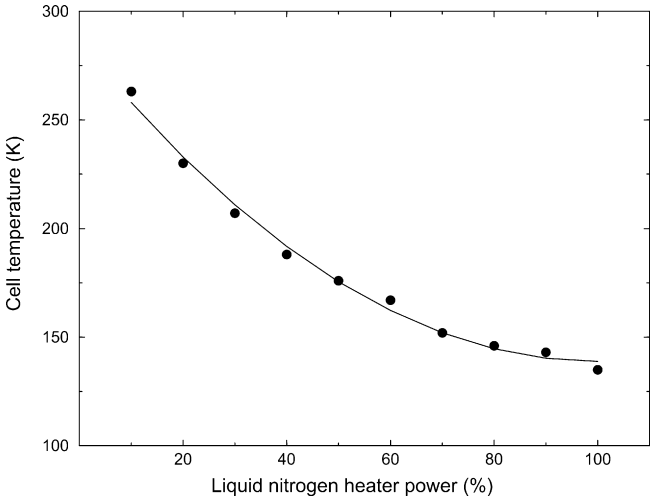

Fig. 5. Stabilized cell temperature as a function of evaporator heater power.

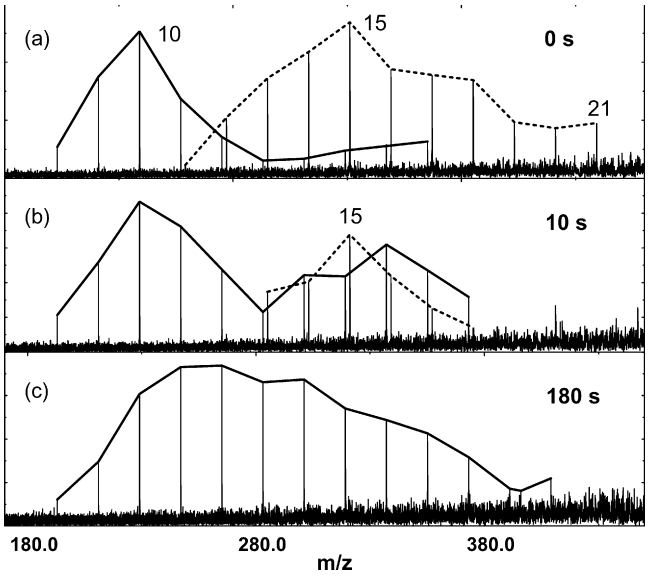

Fig. 6. Temporal evolution of $V^+(H_2O)_n$ (dashed line) and $V^+(OH)_2(H_2O)_{n-2}$ (solid line) at a cell temperature of 89 K. Conversion of $V^+(H_2O)_n$ to $V^+(OH)_2(H_2O)_{n-2}$ is slowed down considerably compared to room temperature, but still takes place. After 180 s, the clusters have apparently kept their size, loss of water molecules has slowed down dramatically.

the cell. The temperature gradient as a function of heater power, shown in Fig. 4, is not constant. It increases with heater power until it reaches a maximum of 5 K at 70%, and then decreases to ~3 K at 100%. The two thermocouples are positioned near the center of the upper and the lower trapping plates, respectively (see Fig. S1). The readings of the lower sensor are higher, because heat is flowing in through the glass ceramics mount which connects the cell to the room temperature flange.

The final stationary cell temperature as a function of heater power is shown in Fig. 5. Using this curve the desired cell temperature can be chosen by an appropriate setting of the evaporator power. The experimental points were fitted using a second-order regression resulting in the curve described by

$$T_{\text{cell}} = 14.7 \times 10^{-3} P_{\text{evap}}^2 - 29.44 \times 10^{-1} P_{\text{evap}} + 285.88$$

Starting at room temperature, the temperature of the ICR cell reaches a stable minimum of 135 K in 3 h. This temperature is maintained with an initially full 20 l Dewar for 4 h, with a maximum drift of 4 K. During the experiments a constant flow of cold nitrogen gas keeps the cell at the desired temperature.

To reach even lower temperatures, the cell can be first precooled using the evaporator. When the minimum temperature with gaseous nitrogen is reached, liquid nitrogen is connected directly to the inlet and circulated through the shield. The cell temperature reaches a value of 89 K and remains stable. During the experiments at this temperature the gradient along the cell was 6.4 K.

During the cooling a significant decrease of the pressure in the ICR cell was seen, since the cold surfaces act as cryo-pumps. For temperatures below 200 K, the pressure drops below 10^{-10} mbar, a side effect which is quite desirable for BIRD studies.

4. Low-temperature BIRD studies of hydrated metal ions

The experiments were performed on a modified Bruker Spectrospin CMS47X mass spectrometer described in detail before [30–32]. Hydrated metal ions $M^+(H_2O)_n$ were produced with an external laser vaporization ion source [33]. The ionic clusters were transferred through several stages of differential pumping into the high-field region of the superconducting magnet, and stored inside the cooled ICR cell at a background pressure of $\leq 10^{-10}$ mbar during 20 cycles. Following accumulation of the ions and mass selection, mass spectra were taken after varying reaction delays.

We have previously studied hydrated vanadium cations $V^+(H_2O)_n$ at room temperature [33,34]. The absorption of black-body radiation induces a competition between several size-dependent processes: loss of water molecules and oxidation to V^{2+} and V^{3+} with formation of atomic and molecular hydrogen, respectively. While for the ions with $n \leq 8$ and $n \geq 24$ only gradual water loss is observed, in the size range $n \approx 9$–24 vanadium is oxidized to V^{3+} and molecular H_2 is formed. Oxidation to V^{2+} and atomic H generation was observed for the clusters for $n = 9$–12. At 300 K the rate constants of these processes are on the order of 0.2–10 s^{-1}, following on average a linear increase with cluster size.

The experiment was repeated, this time with the cell cooled at a temperature of 89 K. The results are shown in Fig. 6. The initial distribution at a nominal $t = 0$ s contains two distributions of equal intensity: hydrated vanadium clusters $V^+(H_2O)_n$, $11 \leq n \leq 21$ and $V(OH)_2{}^+(H_2O)_{n-2}$, $6 \leq n \leq 15$. At low temperatures pure loss of water molecules slows down considerably, while formation of molecular hydrogen accompanied by loss of two or three water molecules persists. It is interesting to note that hydrogen elimi-

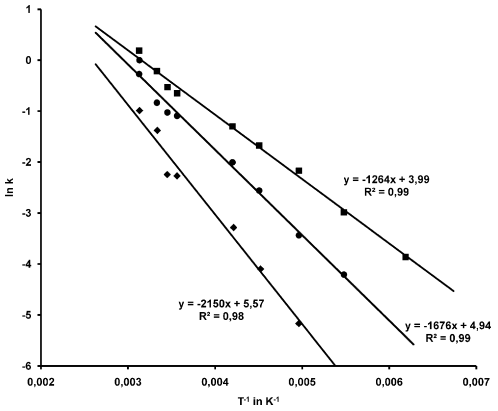

Fig. 7. Arrhenius plots of the BIRD rates of $Ag^+(H_2O)_n$, $n = 4$ (♦), $n = 5$ (●) and $n = 6$ (■), in the temperature range $T = 160$–320 K.

nation seems to occur slowest for the cluster with $n = 15$. Fig. 6b shows the ions present in the cell after 10 s. Most of the initial $V^+(H_2O)_n$ clusters have survived, but with diminished intensity due to the intracluster redox reaction converting them to hydroxide. This seems to be the only reaction channel open at this temperature on the time scale of the experiment. The ions survive even after storing them in the cooled cell for 180 s (Fig. 6c). No water fragmentation is observed even at this long reaction delays, the cooling of the cell walls has effectively stopped this process. The smallest hydroxide cluster in the initial distribution contains eight water molecules and it did not lose any during the 89 K experiment.

The suitability of the cooled cell for quantitative BIRD studies is illustrated in Fig. 7 with the Arrhenius plot of $Ag^+(H_2O)_n$, $n = 4$–6, in the temperature range of 160–320 K. The highest temperature was obtained using heated nitrogen. The lifetimes of the e.g., $n = 6$ clusters against water loss span the range from 1 s at 320 K to 50 s at 160 K. Over this wide temperature range of 160 K, the Arrhenius plot follows a nearly perfect linear behaviour, with $R^2 = 0.9943$.

5. Conclusions and outlook

The strength of our design, with an almost complete enclosure of the cell interior with cooled walls, lies in the well-defined radiation temperature down to at least 160 K, as evidenced by the linear Arrhenius plot of the $Ag^+(H_2O)_6$ ion, while at the same time maintaining a nearly collision-free environment. This is achieved by the use of high heat conductivity ceramics, ample openings in the radiation shield where possible, dynamic trapping without gas assistance and an ion source with a low gas load. It should be noted that in low-temperature BIRD, exchange of radiation is so inefficient that collisions may cause a measurable increase of the dissociation rate even in the lower 10^{-10} mbar range. Another application of the cooled cell is the investigation of ion–molecule reactions under variable and well-defined collision-gas temperatures.

Acknowledgements

Financial support from the Deutsche Forschungsgemeinschaft, the Fonds der Chemischen Industrie, and the European Union in the Research Training Network “Reactive Intermediates Relevant in Atmospheric Chemistry and Combustion” as well as financial support in form of equipment from Bruker Daltonics is gratefully acknowledged. We thank Mirko Gruber and Matthias Stecher for their contribution to data acquisition.

Appendix A. Supplementary data

Supplementary data associated with this article can be found, in the online version, at doi:10.1016/j.ijms.2008.09.001.

References

[1] D. Thölmann, D.S. Tonner, T.B. McMahon, J. Phys. Chem. 98 (1994) 2002.
[2] M. Sena, J.M. Riveros, Rapid Commun. Mass Spectrom. 8 (1994) 1031.
[3] R.C. Dunbar, J. Phys. Chem. 98 (1994) 8705.
[4] P. Weis, O. Hampe, S. Gilb, M.M. Kappes, Chem. Phys. Lett. 321 (2000) 426.
[5] T. Schindler, C. Berg, G. Niedner-Schatteburg, V.E. Bondybey, Chem. Phys. Lett. 250 (1996) 301.
[6] P.D. Schnier, W.D. Price, R.A. Jockusch, E.R. Williams, J. Am. Chem. Soc. 118 (1996) 7178.
[7] W.D. Price, P.D. Schnier, E.R. Williams, J. Phys. Chem. B 101 (1997) 664.
[8] R.C. Dunbar, T.B. McMahon, Science 279 (1998) 194.
[9] B.S. Fox, M.K. Beyer, V.E. Bondybey, J. Phys. Chem. A 105 (2001) 6386.
[10] E.N. Kitova, D.R. Bundle, J.S. Klassen, J. Am. Chem. Soc. 124 (2002) 5902.
[11] A.S. Lemoff, M.F. Bush, E.R. Williams, J. Am. Chem. Soc. 125 (2003) 13576.
[12] R.L. Wong, E.R. Williams, J. Phys. Chem. A 107 (2003) 10976.
[13] S.M. Stevens, R.C. Dunbar, W.D. Price, M. Sena, C.H. Watson, L.S. Nichols, J.M. Riveros, D.E. Richardson, J.R. Eyler, J. Phys. Chem. A 108 (2004) 9892.
[14] R.L. Wong, K. Paech, E.R. Williams, Int. J. Mass Spectrom. 232 (2004) 59.
[15] A.S. Lemoff, M.F. Bush, E.R. Williams, J. Phys. Chem. A 109 (2005) 1903.
[16] W.D. Price, P.D. Schnier, R.A. Jockusch, E.F. Strittmatter, E.R. Williams, J. Am. Chem. Soc. 118 (1996) 10640.
[17] R.C. Dunbar, Mass Spectrom. Rev. 23 (2004) 127.
[18] R.L. Wong, E.W. Robinson, E.R. Williams, Int. J. Mass Spectrom. 234 (2004) 1.
[19] M. Sena, J.M. Riveros, J. Phys. Chem. A 101 (1997) 4384.
[20] M. Sena, J.M. Riveros, Int. J. Mass Spectrom. 227 (2003) 135.
[21] W.D. Price, P.D. Schnier, E.R. Williams, Anal. Chem. 68 (1996) 859.
[22] X.H. Guo, M. Duursma, A. Al-Khalili, L.A. McDonnell, R.M.A. Heeren, Int. J. Mass Spectrom. 231 (2004) 37.
[23] X.H. Guo, M.C. Duursma, A. Al-Khalili, R.M.A. Heeren, Int. J. Mass Spectrom. 225 (2003) 71.
[24] R.D. Leib, W.A. Donald, M.F. Bush, J.T. O'Brien, E.R. Williams, J. Am. Chem. Soc. 129 (2007) 4894.
[25] M.F. Bush, R.J. Saykally, E.R. Williams, Int. J. Mass Spectrom. 253 (2006) 256.
[26] A.S. Lemoff, C.C. Wu, M.F. Bush, E.R. Williams, J. Phys. Chem. A 110 (2006) 3662.
[27] A.S. Lemoff, E.R. Williams, J. Am. Soc. Mass Spectrom. 15 (2004) 1014.
[28] P. Caravatti, M. Allemann, Org. Mass Spectrom. 26 (1991) 514.
[29] LabView 6.0., National Instruments Corporation, Austin, USA.
[30] C. Berg, T. Schindler, G. Niedner-Schatteburg, V.E. Bondybey, J. Chem. Phys. 102 (1995) 4870.
[31] M. Beyer, C. Berg, H.W. Görlitzer, T. Schindler, U. Achatz, G. Albert, G. Niedner-Schatteburg, V.E. Bondybey, J. Am. Chem. Soc. 118 (1996) 7386.
[32] O.P. Balaj, I. Balteanu, B.S. Fox-Beyer, M.K. Beyer, V.E. Bondybey, Angew. Chem. Int. Ed. 42 (2003) 5516.
[33] B.S. Fox, I. Balteanu, O.P. Balaj, H.C. Liu, M.K. Beyer, V.E. Bondybey, Phys. Chem. Chem. Phys. 4 (2002) 2224.
[34] M.K. Beyer, Mass Spectrom. Rev. 26 (2007) 517.